Article

Modeling and Analysis of Entropy Generation in Light Heating of Nanoscaled Silicon and Germanium Thin Films

José Ernesto Nájera-Carpio [1], Federico Vázquez [2,*] and Aldo Figueroa [2]

[1] Instituto de Energías Renovables, Universidad Nacional Autónoma de México, Privada de Xochicalco S/N, Temixco 62588, Morelos, Mexico; E-Mail: najerarpio@gmail.com

[2] Centro de Investigación en Ciencias, Universidad Autónoma del Estado de Morelos, Av. Universidad 1001, Col. Chamilpa, Cuernavaca 62209, Morelos, Mexico; E-Mail: alfil@uaem.mx

* Author to whom correspondence should be addressed; E-Mail: vazquez@uaem.mx; Tel.: +52-777-329-7020; Fax: +52-777-329-7040.

Abstract: In this work, the irreversible processes in light heating of Silicon (Si) and Germanium (Ge) thin films are examined. Each film is exposed to light irradiation with radiative and convective boundary conditions. Heat, electron and hole transport and generation-recombination processes of electron-hole pairs are studied in terms of a phenomenological model obtained from basic principles of irreversible thermodynamics. We present an analysis of the contributions to the entropy production in the stationary state due to the dissipative effects associated with electron and hole transport, generation-recombination of electron-hole pairs as well as heat transport. The most significant contribution to the entropy production comes from the interaction of light with the medium in both Si and Ge. This interaction includes two processes, namely, the generation of electron-hole pairs and the transferring of energy from the absorbed light to the lattice. In Si the following contribution in magnitude comes from the heat transport. In Ge all the remaining contributions to entropy production have nearly the same order of magnitude. The results are compared and explained addressing the differences in the magnitude of the thermodynamic forces, Onsager's coefficients and transport properties of Si and Ge.

1. Introduction

The study of transport phenomena and irreversible processes is necessary in the development of many technological devices. Multilayer systems are involved, for instance, in the development of new type of coats which have application as glues, filters, among others, as well as in thermoelectrics, optoelectronics, solar cells, thermal barriers, mirrors, *etc.* The effects of light incidence in some applications must be understood in order to know how heating affects the performance of the device. Secondary mirrors are used in solar energy concentration devices where high concentrated solar radiation heats them degrading their physical properties. An alternative to reduce heat flow in this process are photonic crystals which can be designed by minimizing the transferring of energy to the structure [1]. Semiconductor technology is being used to exploit the waste heat from various household and industrial processes as in electronic, automotive, and other industries. Development of new thermoelectric materials for that purpose has been rapid in past few years. The analysis of entropy production is being used to characterize materials as, for instance, in the case of ferromagnetic materials under the application of oscillating electromagnetic fields [2] or in the case of thermoelectric materials in thermal oscillating regimes [3,4]. The study of dissipation and irreversibility in different processes in physics and engineering is in the above context a useful tool to found optimization procedures. The minimum entropy production principle states that a system evolves in time reaching a minimum entropy production rate at the stationary state. This often establishes a relation between irreversible processes and optimal performance [5,6]. The investigation of these relationships in dielectric thin films constitutes the foundation of the understanding of behavior and performance of multilayer systems. This theme has attracted the interest of the scientific community [7–10] and it is the one we are interested in.

In this work, we address the problem of light heating of Si and Ge thin films and study in detail the contributions to the entropy production in the system. This involves irreversible processes associated with heat transferring, particle transport and generation of electron-hole pairs via light-matter interaction. The main interest in considering Si and Ge is due to their importance as constituent materials in the field of quantum dots, quantum wires and quantum wells [11]. Here, we quantify and compare the entropy generation as produced by dissipative fluxes both in the case of Silicon and Germanium thin films. We explain differences in terms of the transport properties of each material as well as the magnitude of thermodynamic forces producing fluxes. The modeling is based on balance equations of mass and energy obtained from fundamental principles of irreversible thermodynamics. They are solved by using a high order numerical method, the so called Spectral Chebyshev Collocation method [12,13], in order to validate solutions obtained from *Wolfram Mathematica 10.0*. The survey is as follows. In Section 2 we include a description of the physical model used to study the dissipative processes and entropy production in a semiconductor film. The model is obtained from basic principles of irreversible thermodynamics by means of a suitable choosing of thermodynamic forces and fluxes.

This leads to identify six processes producing entropy in the system related with the heat transport. They are particle transport and generation-recombination of electron-hole pairs, besides the absorption of light in the medium through two mechanisms, namely, the generation of electron-hole pairs and the transferring of energy from the incident light to the lattice. The Chebyshev Collocation method is described at the end of this section. Our results concerning the stationary profiles of heat flux, particle density distributions and generation-recombination pairs rate as well as the associated entropy production to each dissipative process can be seen in Section 3, where it is also included a discussion focused to the understanding of the differences in the contributions to entropy production for Si and Ge. We end the article with some concluding remarks in Section 4.

2. Methods

2.1. The System

The considered system is schematically shown in Figure 1. It consists of a thin film (in grey) of Si (Ge) with thickness L. The incidence of the light beam is from the left as it can be seen. Air is assumed to the left of the film and a heat and particle source to the right. This last may be conceived like a substrate at constant temperature which conducts charged particles. In the left boundary we suppose that the film radiates energy at temperature $T(0)$ and losses heat by convection. In the right boundary the temperature is fixed with value $T(L) = T_0$ and $n(L) = n_0(T_0)$, $p(L) = p_0(T_0)$, where n_0 and p_0 are the electron and hole densities at the fixed value of temperature T_0. Initial conditions are represented by uniform distributions of temperature and particle densities.
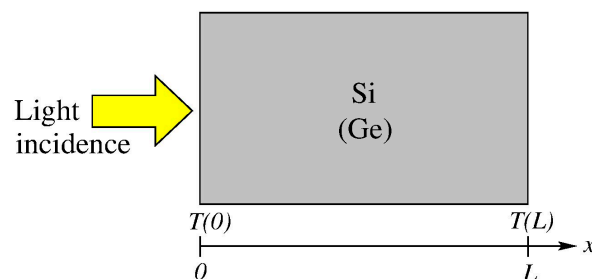

Figure 1. A schematic view of a Si (Ge) thin film of length L with incidence of light from the left.

2.2. Mathematical Model

Due to the progress in the microscaling techniques the film thickness may be reduced to become comparable to the phonon mean free path (PMFP). When the thickness is below the PMFP the heat and charged particles transport regime becomes of the ballistic type. This may make necessary to use a radiative transport equation to describe energy transfer [14]. Otherwise, the transport pertains mainly to the diffusive regime. In this work, the film thickness of the film is constrained to be above the PMFP in such a way that the classical constitutive equations together with continuity and energy conservation equations represent a valid autonomous mesoscopic theory to describe heat and particle transport in the system. Combination of the internal energy conservation and the continuity equations for electron and holes densities with suitable constitutive equations leads to a transport model where

the incident light energy is incorporated as a volumetric heat source to account for the absorption of energy by the medium. The three so obtained equations can be solved with the above boundary conditions for the temperature and the particle densities to obtain the space distribution of quantities of interest.

We then start by stating the basic assumptions made to formulate the governing equations of densities and fluxes [15]: (a) The system is considered as constituted by the host lattice (a particle and heat conductor rigid solid) and two species, namely, electrons and holes subjected to drift and diffusion. This system is denoted here on as LEH. The lattice is assumed to be non-magnetizable; (b) Each of the three components (lattice, electrons and holes) is locally in thermodynamic equilibrium; (c) They are able to interchange energy with each other by various scattering mechanisms; (d) The three components are in thermal equilibrium; (e) The admissible states of electrons and holes are determined by their particle densities and chemical potentials, as well as the local equilibrium temperature. For the case of the host lattice its physical states are defined solely by its temperature; (f) The internal electric energy is of electrostatic nature and the associated field is given by Poisson equation (Equation (A32) below). The electric potential ϕ is not a dynamic variable. For a more detailed discussion about this point see [15]; (g) The whole system is thermally coupled to the ambient and the electromagnetic field of the incident light.

Some comments on condition d) are in order. The thermal equilibrium among species in the system is reached if one assumes that electrons in the conduction band do not have enough energy to produce effects such as tunneling and others, but they only stay in the conduction band and then recombine with holes. This assumption is supported by the fact that there are no externally applied high electric fields that could provide the energy needed for the electrons tunnel out of the material. This led us to write the particle flows with constant mobility and diffusion coefficients. In this situation, both the lattice and the populations of electrons and holes are not far from the equilibrium, which allows us to assume that they are in thermal equilibrium with the lattice. It must be noted that inhomogeneities in the electron density and local cross effects in the system (as Seebeck's) make the electrons in the conduction band flow during the time they stay in the conduction band.

The model derived from the above assumptions is obtained along basic principles of irreversible thermodynamics. In order to make this paper self-contained the thermodynamic formalism is exposed in detail in Appendix A (see also [16]).

2.3. The Reduced Model

The resulting equations are very complicated and highly non-linear. They were simplified through a dimensional analysis. The final form of the dynamic equations used to describe heat and particle transport can be seen below in Equations (1)–(3). They were obtained from Equations (A1) and (A2) and (A34) with Equations (A26)–(A28) and (B1) and the dimensional analysis found in Appendix C. The continuity and energy conservation dimensional equations for the stationary state read as follows:

$$K_B L_{11} T(x) \left(\frac{\partial n}{\partial x} \right)^2 - 2K_B L_{11} n(x) \frac{\partial T}{\partial x} \frac{\partial n}{\partial x} + K_B L_{11} T(x) n(x) \frac{\partial^2 n}{\partial x^2}$$

$$- \left(L_{13} + K_B L_{11} Log \left(\frac{n}{N_c} \right) \right) n(x)^2 \frac{\partial^2 T}{\partial x^2} = 0, \tag{1}$$

$$- K_B L_{21} T(x) \left(\frac{\partial p}{\partial x} \right)^2 + 2K_B L_{21} p(x) \frac{\partial T}{\partial x} \frac{\partial p}{\partial x} + K_B L_{21} T(x) p(x) \frac{\partial^2 p}{\partial x^2}$$

$$- \left(L_{23} - K_B L_{21} Log \left(\frac{p}{N_v} \right) \right) p(x)^2 \frac{\partial^2 T}{\partial x^2} = 0, \tag{2}$$

$$L_{35} \frac{\partial^2 T}{\partial x^2} + P = 0, \tag{3}$$

where $n(x)$ and $p(x)$ are the particle densities of electrons and holes, respectively, $T(x)$ is the thermal equilibrium temperature of the electrons, the holes and the lattice. The quantities L_{ij} are Onsager's coefficients described in Appendix A, while $P(x)$ is the energy of incident light transferred as heat to the lattice. K_B is the Boltzmann's constant. It is worth mentioning that in the stationary state the generation rate of electron-hole pairs equals the net recombination rate, *i.e.*, $R - G = 0$. This is the reason why the term $R - G$ does not appear in Equations (1) and (2). The complete reduced equations can be seen in Appendix C.

The potential function ϕ of the self-consistent electric field is given by Poisson's Equation, transcribed here from Appendix A:

$$\frac{\partial}{\partial x} \left(\varepsilon \frac{\partial \phi}{\partial x} \right) = q(n - p) \tag{A32}$$

In the next section we establish the boundary conditions accompanying Equations (1)–(3).

2.4. Boundary Conditions

Boundary conditions (b.c.) for temperature and particle densities have been extensively studied [17–19]. We assume here radiation and convective b.c. for the temperature equation, Equation (3), at the left hand side of the film and Dirichlet b.c. at the right hand side. The last implies that the system is in contact with a heat and particle reservoir at a constant temperature T_0 at $x = L$. The thermal b.c. are then written as:

$$K \frac{\partial T}{\partial x} \bigg|_{x=0} = h \left(T(0) - T_\infty \right) + \varepsilon \sigma \left(T(0)^4 - T_\infty{}^4 \right) \tag{4}$$

$$T(L) = T_0 \tag{5}$$

In expression (4), h is the convection coefficient of the air surrounding the thin film on the left and ε and σ the emissivity of the material and the Stephan-Boltzmann constant, respectively.

For the particle density equations, Equations (1) and (2), zero particle flux is assumed at the left hand side of the film while at the right hand side b.c. are $n(L) = n_0(T_0)$ and $p(L) = p_0(T_0)$. These conditions read as follows (see Equations (A26) and (A27) in Appendix A)

$$\left(L_{11}\frac{\partial v_n}{\partial x} - L_{12}E_x - L_{13}\frac{\partial T}{\partial x} \right)\Bigg|_{x=0} = 0,$$

$$\left(-L_{21}\frac{\partial v_p}{\partial x} + L_{22}E_x - L_{23}\frac{\partial T}{\partial x} \right)\Bigg|_{x=0} = 0 \tag{6}$$

$$n(L) = N_c e^{-\frac{E_g}{2K_B T_0}}$$

$$p(L) = N_v e^{-\frac{E_g}{2K_B T_0}} \tag{7}$$

As it can be seen, the electron and hole densities have been written in terms of their equilibrium values at temperature T_0 in $x = L$. In Equations (6) and (7) N_c and N_v are the densities of states in the conduction and the valence band, respectively, and E_g is the gap energy of the material. Note that, as it can be shown, the continuity equations do not support a finite solution if the particle fluxes are zero at both sides of the film and therefore the steady state for particle densities does not exist. This is due to the fact that the incident light acts as a continuous source of particles in the system and the walls would be preventing the passage of particles outside. Finally, the b.c. for the electric potential ϕ in Poisson equation, Equation (A32), is taken of Dirichlet type [20]. This condition fixes the zero level of electric potential energy at the film walls. It is given as

$$\phi(0) = \phi(L) = 0. \tag{8}$$

2.5. Solutions for n, p and T

In this short section, we describe how the solutions of the stationary Equations (1)–(3) with b.c. Equations (4)–(8) are obtained. First we note that the temperature field becomes decoupled from Equations (1) and (2). We then find an analytical solution of Equation (3) for the stationary state, obtained with *Wolfram Mathematica 10.0*, where the source term is taken from Equations (B1). It reads

$$T(x) = k_{0T} + k_{1T}e^{-ax} + k_{2T}e^{-bx} + k_{3T}x \tag{9}$$

For numerical values of the constants in the above equation see Appendix D. Afterwards the continuity Equations (1) and (2) are numerically solved for n and p with *Mathematica* and the solutions validated with a high order numerical method described in the next subsection.

2.6. Spectral Chebyshev Collocation Method

The numerical method used here is based on the Spectral Chebyshev Collocation (SCC) method which assumes that an unknown Partial Differential Equation (PDE) solution can be represented by a global, interpolating, Chebyshev partial sum. This form is often convenient, particularly if the solution is required for some other calculation where its rapid and accurate evaluation is important. In a finite-difference method, the approximation of a derivative at a grid point involves only very few neighboring grid values of the function, while the Chebyshev approximation involves all the grid values. The global character of spectral methods is beneficial for accuracy. Once the finite Chebyshev series representing the solution is substituted into the differential equation the coefficients are determined so that the differential equation is satisfied at certain points within the range under

consideration. In this spectral method, the PDE equation is required to be satisfied exactly at the interior points, namely, the Gauss-Lobatto collocation points given by

$$x_i = \cos\left(\frac{i\pi}{N}\right) \tag{10}$$

with $i = 1,..., N-1$.

In Equation (10), N denotes the size of the grid. The number of points is chosen so that, along with the initial or boundary conditions, there are enough equations to find the unknown coefficients. The positions of the points in the range are chosen to make small the residual obtained when the approximate solution is substituted into the differential equation. The range in which the solution is required is assumed finite, and, for convenience, a linear transformation of the independent variable is made to make the new range $(-1, 1)$.

Finally, an additional property of the spectral methods is the easiness with which the accuracy of the computed solution can be estimated. This can be done by simply checking the decrease of the spectral coefficients. There is no need to perform several calculations by modifying the resolution, as is usually done in finite-difference and similar methods for estimating the "grid-convergence". A further explanation of this spectral method can be found in [12,13].

The spatial derivative terms in Equations (1) and (2) were expressed on derivative matrices expanded on Chebychev polynomials. The matrix-diagonalization method was used to solve the coefficient equation system in physical space directly. A coordinate transformation was necessary either to map the computational interval to $-1 < x < 1$.

In Section 3 we report and discuss our results concerning the temperature and particle density profiles in the stationary state as well as the contributions to the entropy production.

3. Results and Discussions

In this section, our main results are displayed and discussed. They were obtained by using the values for Silicon (Si) and Germanium (Ge) parameters given in Table 1 and Appendix D. The assumed value of the electric field of the incident light is $E_0 = 613.99 \, N/C$ which corresponds to the intensity of the solar light on earth. The film thickness is $100 \, nm$. The convection coefficient of the air surrounding the thin film on the left is taken as $h = 5 \, W/m^2 K$ and the emissivity ε is 0.88 and 0.09 for Si and Ge, respectively. Finally, the reference temperature is $T_0 = 330 \, K$.

Table 1. Values of physical constants. K_0 is the thermal conductivity, ρ is the thermal resistivity, g_n and g_p are electric conductivities of electrons and holes, respectively, E_g is the gap energy, α is the absorption coefficient and η is the refractive index.

Material	K_0 (W/mK)	ρ (mK/W)	g_n $(1/m\Omega)$	g_p $(1/m\Omega)$	E_g (eV)	α $(1/m)$	η
Si	148	0.0067	0.0002	0.00003	1.12	1×10^7	4.01
Ge	59.9	0.0167	1.601	0.47	0.66	7×10^7	4.01

In Figure 2, it can be seen the source term $P(x)$ of the energy conservation equation as a function of the position within the material. The x domain has been redefined from $[0, L]$ to $[-1, 1]$ in this and the following figures. P decays much faster in Ge than in Si. In Ge it diminishes almost one order of

magnitude in the first third of the length of the medium, while in Si it decrements more or less a half of one order of magnitude in the whole length of the device. Moreover, in $x = -1$ its magnitude in Ge is greater than in Si by almost one order of magnitude. The behavior of P in the profile allows one to understand some of the following results shown in Figures 3–8.
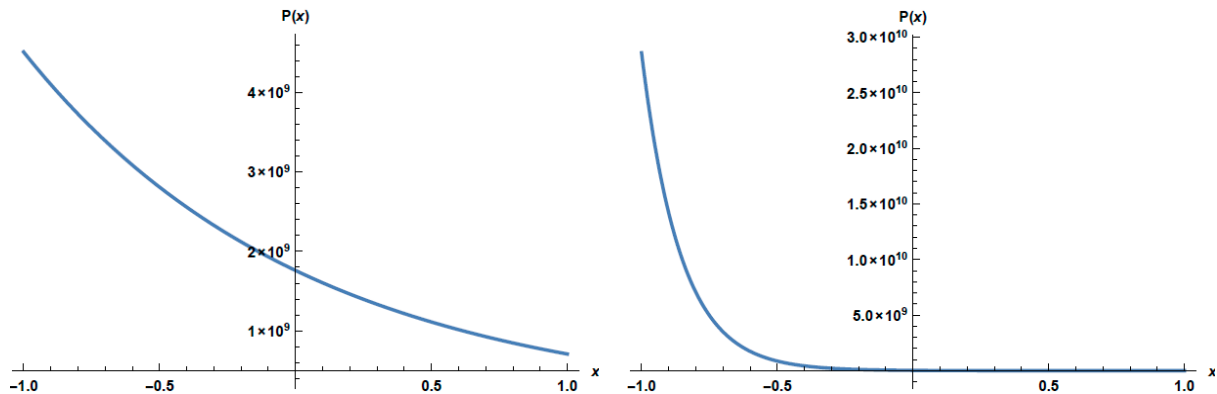

Figure 2. Absorbed light converted in heat *vs.* the position in the profile as given by the source term P $\left(1/m^3\right)$ in Equation (B1). Si (**left**) and Ge (**right**).
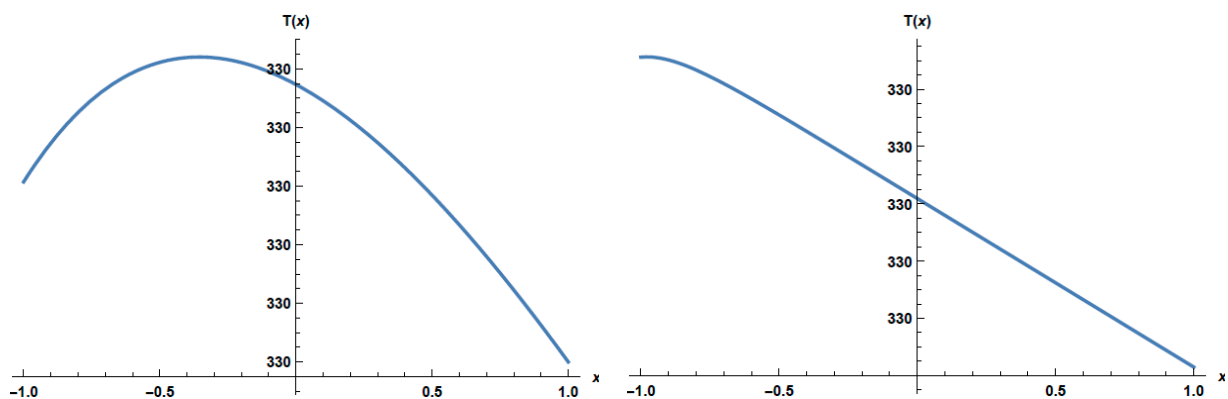

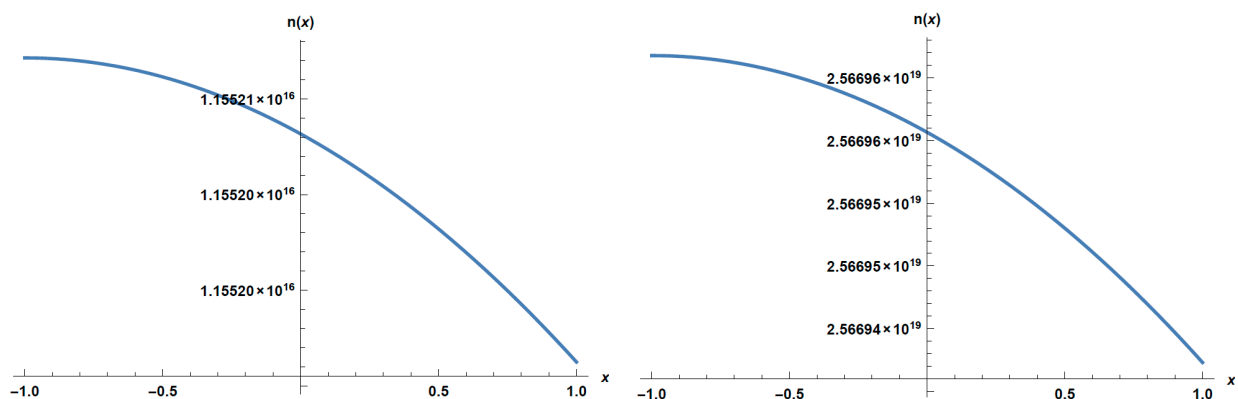**Figure 3.** Stationary temperature (K) profiles for Si (**left**) and Ge (**right**).

Figure 4. Stationary electron density $\left(1/m^3\right)$ profile for Si (**left**) and Ge (**right**).

In Figure 3, we present the stationary temperature profile for Si (left) and Ge (right) films. We remark the parabolic-like form of the profile in both cases. As mentioned, $T(x)$ was obtained by analytically solving Equation (3) in the stationary state with the b.c. (4) and (5). The temperature in the

profile is strongly influenced by $P(x)$ in the energy conservation equation. The displacement of the maximum of temperature to the left in both cases (Si and Ge) is due to the decaying behavior of $P(x)$ shown in Figure 2.
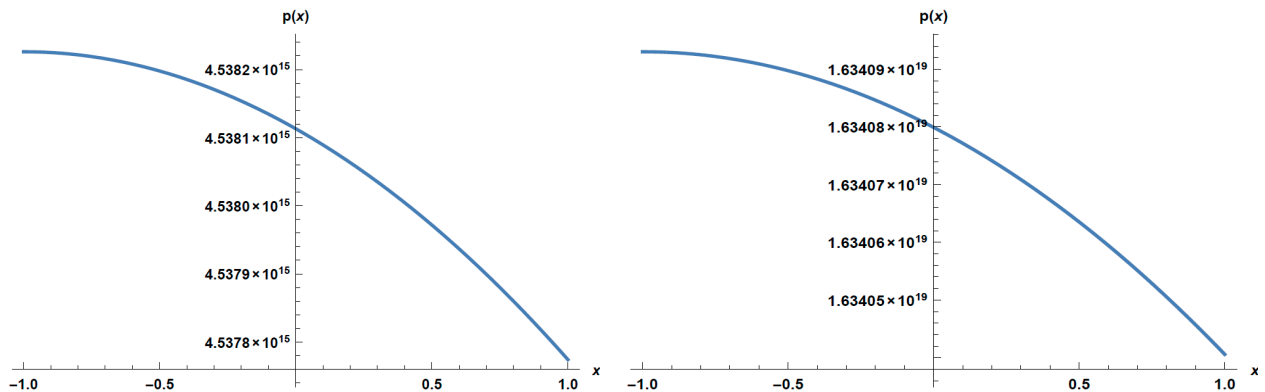
Figure 5. Stationary hole density $\left(1/m^3\right)$ profile for Si (**left**) and Ge (**right**).
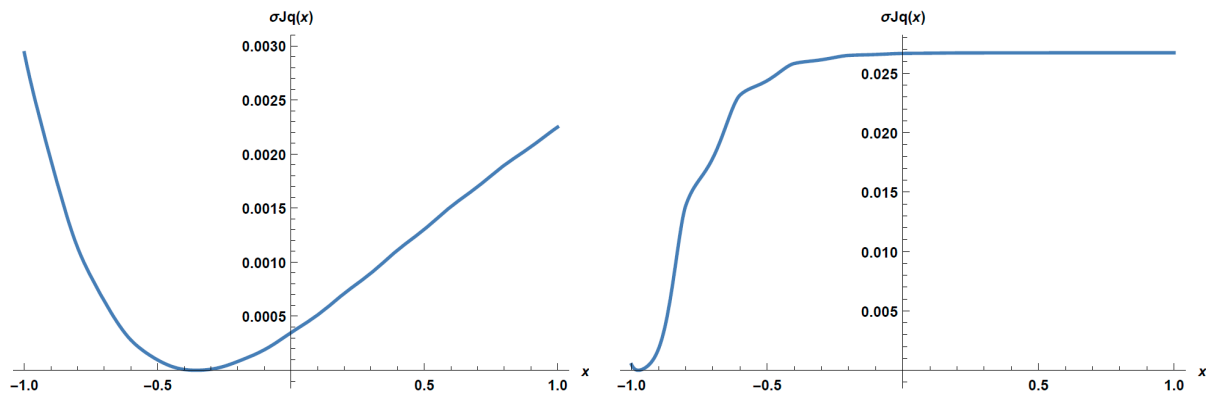
Figure 6. Distribution in the profile of entropy production $\left(J/Km^3s\right)$ from heat transport. The figure on the left corresponds to Si and that on the right to Ge.
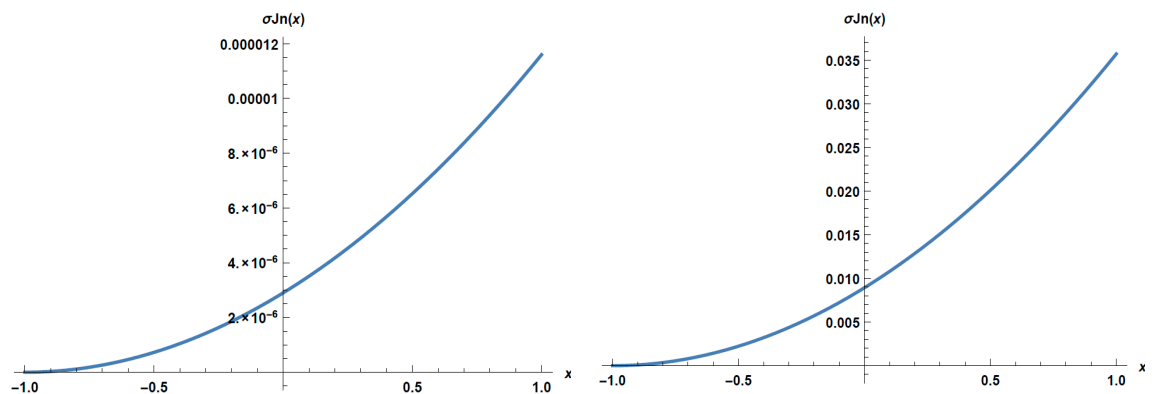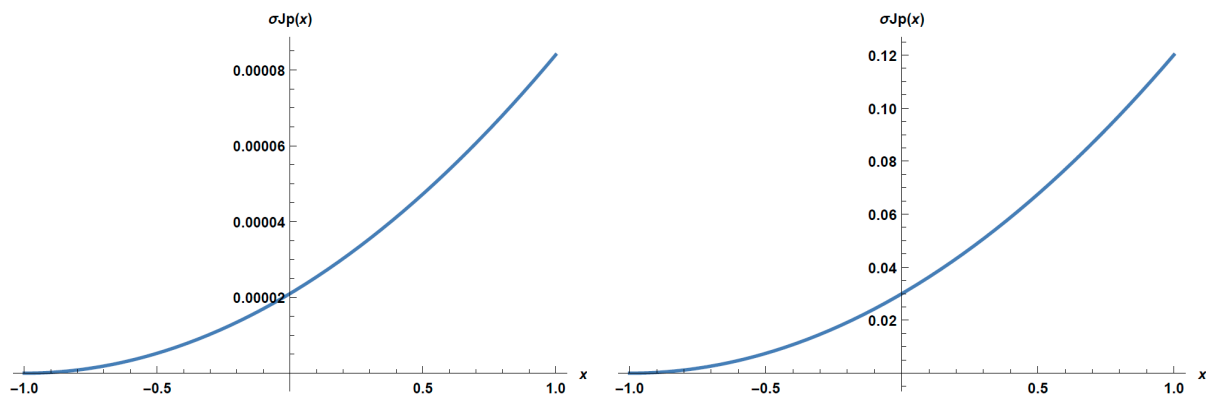
Figure 7. *Cont.*

Figure 7. Entropy produced $\left(J/Km^3s\right)$ by particle transport processes in Si (**left**) and Ge (**right**). Above it can be seen the entropy production due to electron flux and below that due to hole flux.
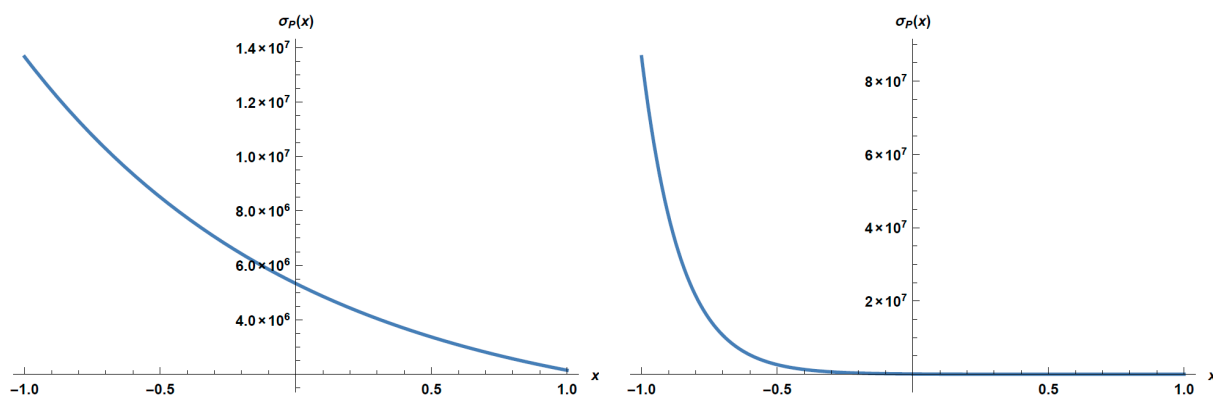

Figure 8. Entropy production $\left(J/Km^3s\right)$ from the interaction of the incident light with the material. The figure on the left corresponds to Si and those on the right to Ge.

The stationary electron densities in the profile can be seen in Figure 4 where the left graph corresponds to Si and that on the right to Ge. They were obtained by solving Equation (1) in the stationary state. It can be seen how the temperature gradient produces a redistribution of the electron density in the profile.

In Figure 5 it can be seen the stationary hole densities in the profile. The figure on the left corresponds to Si and that on the right to Ge. The displacement of the maximum density to the left in the case of Ge is due to the extreme position of its maximum temperature as seen in Figure 3. Ultimately this is a result of the spatial distribution of the light energy transferred to the lattice as inner energy.

Note that the electron and hole densities for Ge are bigger by a factor of 10^3 and of 10^4 than those for Si, respectively. This can be understood in terms of the difference in the gap energy in Ge which is smaller than that of Si (see Table 1 above). All the particle profiles shown in Figures 4 and 5 were obtained by solving Equations (1) and (2) with the stationary profile of the temperature in the system and b.c. (6) and (7) for the particle densities and (8) for the electric potential.

A few words on the dissipative flows are appropriate at this point. The result obtained for the heat flux from the numerical temperature distribution (Equation (C3)) shows that it is directed outwards the device in the part of the spatial domain to the left of the maximum temperature. On the right of this

maximum, it is also directed outwards. This behavior is found for both Si and Ge. Moreover, in the case of Ge a constant positive value is observed in practically the whole right part of the domain. The electron and hole fluxes have a different behavior. The electrons flow toward the left side in all the domain of the film while the holes flow towards the constant temperature side. In this way, the fluxes oppose one another in the spatial domain. The generation-recombination of electron-hole pairs vanishes in the whole domain as a consequence of the stationary condition, namely $-R + G = 0$.

Our next graphs concern the contributions to the entropy production from different dissipative processes. They can be seen in Figures 6–8, where the cases of Silicon and Germanium have been plotted on the left and on the right respectively. We begin with the entropy produced by the heat flux in Figure 6. Both graphs have a minimum entropy production which coincides with the position of the maximum temperature in the profile (Figure 3) where the heat flux vanishes.

The entropy produced by the transport of electrons and holes through the lattice for both Si and Ge can be seen in Figure 7. As appreciated in the figure, the entropy production due to the particle fluxes is $O(10^{-5})$ for electron flux in the case of Si, while it is $O(10^{-2})$ for Ge; for holes they are $O(10^{-5})$ and $O(10^{-1})$, respectively. The outstanding differences among the respective entropy productions can be explained if one considers two facts: first, the magnitude of the entropy production is mostly determined by the term in the chemical potential derivative in Equations (A26) and (A27) for electrons and holes. From this it is inferred that the entropy production is determined by the coefficients L_{11} and L_{21} for electrons and holes, respectively. Accordingly with Appendix D L_{11} and L_{21} for Ge are bigger by a factor of 10^4 than the values of the same coefficients for Si. It is worth mentioning the fact that the entropy production increases toward the constant temperature side in all cases. This is explained by the fact that the particle flux also increases toward the same side.

In Figure 8, we show the entropy produced by the interaction of the light with matter transferring energy to the lattice. Clearly, it dominates over all other dissipative processes in the LEH system by almost 10 orders of magnitude. The spatial distributions nearly follow the shape of the spatial distributions of the source term P in Figure 2. The final figure of this sequel is that of the partial entropy production defined as

$$\sigma_{PARTIAL} = \sigma_{Jq} + \sigma_{Jn} + \sigma_{Jp} + \sigma_{RG} \tag{11}$$

This can be seen in Figure 9, where it was plotted by omitting the contribution of the entropy produced by the light-matter interaction. If this last is included, the graphs look like the graphs of the entropy production due to the transferring of energy from light to the lattice (Figure 8) hiding the contribution of all other dissipative effects. Anyway, they adopt the general features of the dominant contribution, *i.e.*, the entropy produced by heat transport in the case of Si and the joint effect of all the contributions in the case of Ge.
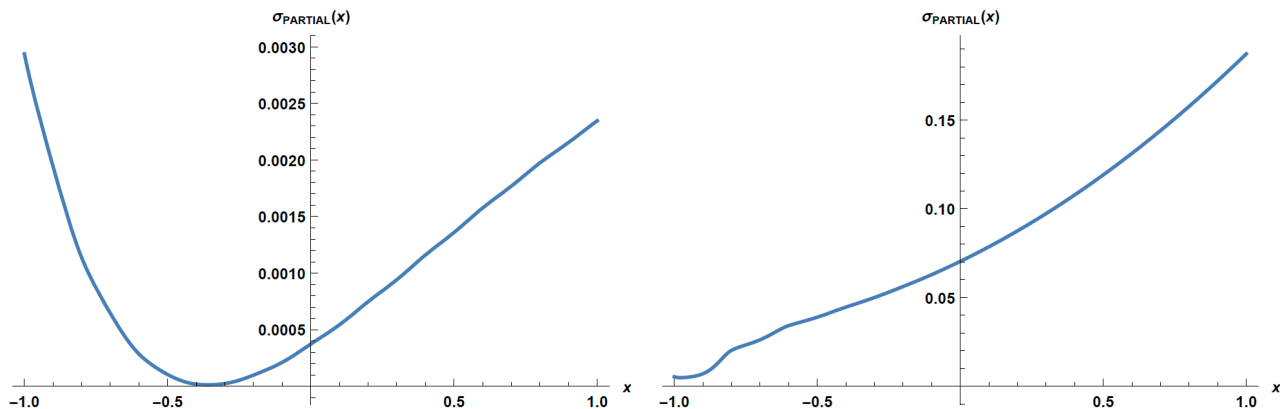
Figure 9. Partial entropy production (Equation (11)) in the profile (it does not includes the interaction light-matter processes) for Si (**left**) and Ge (**right**). The entropy production is in $\left(J / Km^3 s \right)$.

We finalize this section by showing the global values (the entropy is integrated in the spatial domain) of the contributions to entropy production and the total value of it for Si and Ge. Table 2 contains the data of such values corresponding to heat flux, electron and holes fluxes and generation-recombination processes, light energy conversion in heat, as well as the total entropy production without the contribution due to the light energy conversion.

Table 2. Comparison of global contributions to the entropy production from different dissipative processes: Heat flux (J_q), electron flux (J_n), hole flux (J_p), electron-hole generation-recombination processes (R and G) and conversion of energy light in heat (P). It is also included the electron and hole mean densities.

Material	$\sigma_{Jq_{global}}$ $\left(\dfrac{J}{Km^3 s} \right)$	$\sigma_{Jn_{global}}$ $\left(\dfrac{J}{Km^3 s} \right)$	$\sigma_{Jp_{global}}$ $\left(\dfrac{J}{Km^3 s} \right)$	σ_{RG} $\left(\dfrac{J}{Km^3 s} \right)$	$\sigma_{P_{global}}$ $\left(\dfrac{J}{Km^3 s} \right)$	$\sigma_{Partial_{global}}$ $\left(\dfrac{J}{Km^3 s} \right)$	n_{mean} $\left(\dfrac{1}{m^3} \right)$	p_{mean} $\left(\dfrac{1}{m^3} \right)$
Si	1.891×10^{-3}	7.732×10^{-6}	5.599×10^{-5}	0	1.232×10^{7}	1.959×10^{-3}	1.155×10^{16}	4.538×10^{15}
Ge	4.662×10^{-2}	2.381×10^{-2}	7.999×10^{-2}	0	1.238×10^{7}	1.599×10^{-1}	2.567×10^{19}	1.634×10^{19}

4. Conclusions

In this final section, some further comments are included. First, we would like to comment on the experimental support needed for any theoretical whose aim is to describe a physical phenomenon. Next, we try to justify our numerical model and finally we make general comments on our results.

Up to the best of the author's knowledge there are not experimental observations that can be used to support the results obtained in this work. In fact, this work has been conceived to motivate experimentalists to address the problem of the use of entropy production criterion to optimize thermal nanostructured devices. Our aim here is to establish a theoretical and numerical basis to address that problem. Nevertheless, the continuity equations in our model (Equations (1) and (2)) admit an analytical solution if the temperature is assumed constant in the domain (as indeed it is). We have

compared the numerical solutions with the analytical one and have found a great agreement. It seems to us that this could justify in some extent the used numerical model.

The following are final comments on our results.

(a) It is noted that the temperatures of Si and Ge depend on several factors but mainly on the temperature of heat source at $x = 1$. As a matter of fact, the profile in both cases shows an almost flat shape due to the contact of the film with the heat source at a temperature T_0. Its spatial distribution is also determined by the magnitude of the absorption coefficient and the energy input due to the incident light at $x = -1$, as well as the b.c. at the same position. (b) We note that all the profiles in Figures 3 to 5 corresponding to the temperature and the particle densities show an extreme value at some position where the fluxes vanish (in fact, for the particle densities this position is at $x = -1$). This is the reason why the corresponding contributions to the entropy production show a minimum (in fact, they vanish) at the same position. c) We refer now to the different contributions to entropy production displayed in Figures 6 to 8 and the global values shown in Table 2. It is seen that the conversion of light energy in heat (P) is the dominant irreversible process in both Si and Ge. After this, the hole transport process is the most important in Ge while in Si is the heat transport. In Ge the remaining contributions (due to heat flux and electron transport) are on the same order of magnitude. In both materials, the smallest contributions to the entropy production are the generation-recombination of electron-hole pairs which vanish by the stationary condition. d) The fact that the entropy production due to particle transport (both electrons and holes) is bigger for Ge than for Si can be understood if one pays attention to the differences in the magnitude of Onsager's coefficients L_{11} and L_{21}. As shown in Appendix D, they are bigger by a factor of 10^4 in Ge than in Si. Their chemical potential gradients are on the same order. e) The entropy produced by heat transport process is bigger in the case of Ge than that of Si. The temperature gradient is responsible for this difference since in the case of Ge it is one order of magnitude bigger than in the case of Si. The thermal conductivities are on the same order. f) The summed global contributions to entropy production excepting those coming from the transferring of the energy of incident light into the material is represented in Table 2 by $\sigma_{Partial_{global}}$.

To conclude, we summarize this work as follows. We have calculated the contributions to the entropy production in Si and Ge thin films with light incidence. The system was considered to be constituted by the lattice and two different species, namely, electrons and holes. The model was based on principles of irreversible thermodynamics. Heat transfer, particle transport and electron-hole generation-recombination processes were included as well as light-matter interaction. The final form of balance and constitutive equations for electron density, holes density, internal energy, heat flux, electron flux, holes flux and recombination processes, respectively, is shown in Appendix A in Equations (A1) to (A8). We have seen that the relative magnitude of thermodynamic forces, Onsager's coefficients and transport coefficients determine and explain the relative magnitude of the contributions to the entropy generation in the two materials considered. The most significant contribution to the entropy production comes from the interaction of light with the medium in both Si and Ge. This interaction includes two processes, namely, the generation of electron-hole pairs and the transferring of energy from the absorbed light to the lattice. The last is the dominant irreversible process in the LEH system for both Si and Ge.

The results contained in this work may be useful to the design of thin films used in electronic industry where the control of irreversible processes is an important issue.

Acknowledgments

Author Contributions

José Ernesto Nájera-Carpio: Conception and design of the study, analysis tools, analysis of the data, interpretation of the data, drafting the article. Federico Vázquez: Conception and design of the study, interpretation of the data, drafting the article, critical revision of the manuscript. Aldo Figueroa: Analysis tools, analysis of the data, critical revision of the manuscript. All authors have read and approved the final manuscript.

Conflicts of Interest

The authors declare no conflict of interest.

Appendix

A. Thermodynamic Formalism

The governing equations of particle densities and internal energies are written in one dimension as [15,16,21,22]:

$$\frac{\partial n}{\partial t} - \frac{\partial J_n}{\partial x} = -R + G \tag{A1}$$

$$\frac{\partial p}{\partial t} + \frac{\partial J_p}{\partial x} = -R + G \tag{A2}$$

$$\frac{\partial u_n}{\partial t} + \frac{\partial J_n^u}{\partial x} = -qEJ_n + P_n \tag{A3}$$

$$\frac{\partial u_p}{\partial t} + \frac{\partial J_p^u}{\partial x} = qEJ_p + P_p \tag{A4}$$

$$\frac{\partial u_L}{\partial t} + \frac{\partial J_L^u}{\partial x} = P_L \tag{A5}$$

where sub-indexes n, p and L denote electrons, holes and lattice, respectively. n, J_n, p and J_p are the electron and the hole number densities and the corresponding particle fluxes, respectively; R is the net recombination rate of electrons and holes by photon transitions, G is the generation of electron-

hole pairs due to the interaction of the incident light with the lattice; E is the self-consistent electric field described through Poisson's equation; it is given in terms of an electrostatic potential function ϕ by $-\partial\phi/\partial x$, and q the electron electric charge. Since the LEH system is coupled to the radiation field of the incident light, internal energy is not conserved. P_n, P_p and P_L are the source terms in the energy balance Equations (A3)–(A5) of the electrons, holes and the lattice, respectively. In Equations (A3)–(A5), u_j and J_j^u ($j=n,p,L$) are the internal energies and the corresponding energy fluxes of electrons, holes and the lattice, respectively. Note that $-R$ describes the total balance of generation and recombination of electron-hole pairs. It must be remembered that a negative value of R means that generation overpasses recombination of electron-hole pairs.

Now we make the fundamental assumption that there exist a set of thermodynamic potentials $S_n = S_n(u_n, n)$, $S_p = S_p(u_p, p)$ and $S_L = S_L(u_L)$, which are identified with the entropy density functions of each of the components of the LEH system. They are defined through the Gibbs relations:

$$T_n dS_n = du_n - v_n dn \tag{A6}$$

$$T_p dS_p = du_p - v_p dp \tag{A7}$$

$$T_L dS_L = du_L \tag{A8}$$

where T_j and v_j ($j=n,p$) are the temperatures and chemical potentials of electrons and holes, respectively. T_L is the temperature of the lattice. We now define the total entropy of the LEH system as

$$S_T = S_n + S_p + S_L \tag{A9}$$

in such a way that by using Equations (A1)–(A8) in the time derivative of Equation (A9) one can arrive to the total entropy density balance equation which reads:

$$\frac{\partial S_T}{\partial t} + \nabla \cdot \left(\frac{J_L^u}{T_L} + \frac{J_n^u}{T_n} + \frac{J_p^u}{T_p} + \frac{v_n J_n}{T_n} - \frac{v_p J_p}{T_p} \right) =$$

$$\frac{J_n}{T_n} \cdot \left(\nabla v_n + q\nabla\varphi \right) + \frac{J_p}{T_p} \cdot \left(-\nabla v_p - q\nabla\varphi \right) + J_L^u \cdot \nabla\left(\frac{1}{T_L} \right) + J_n^u \cdot \nabla\left(\frac{1}{T_n} \right) + J_p^u \cdot \nabla\left(\frac{1}{T_p} \right)$$

$$+ v_n J_n \cdot \nabla\left(\frac{1}{T_n} \right) - v_p J_p \cdot \nabla\left(\frac{1}{T_p} \right) + \left(R - G \right)\left(\frac{v_n}{T_n} + \frac{v_p}{T_p} \right) + \frac{P_L}{T_L} + \frac{P_n}{T_n} + \frac{P_p}{T_p} \tag{A10}$$

Let us introduce the electrochemical potentials $\overset{\wedge}{\phi}_n$ and $\overset{\wedge}{\phi}_p$ of electrons and holes through the expressions:

$$\overset{\wedge}{\phi}_n = v_n + q\phi \tag{A11}$$

$$\overset{\wedge}{\phi}_p = -v_p - q\phi \tag{A12}$$

By assuming local thermal equilibrium among the components of the system LEH, *i.e.*,

$$T_L = T_n = T_p = T \tag{A13}$$

one can rewrite Equation (A10) as:

$$\frac{\partial S_T}{\partial t} + \nabla \cdot J_T^S = \frac{J_n}{T} \cdot \nabla \hat{\varphi}_n + \frac{J_p}{T} \cdot \nabla \hat{\varphi}_p + J_q \cdot \nabla\left(\frac{1}{T}\right) + (R-G)\left(\frac{\nu_n + \nu_p}{T}\right) + \frac{P}{T} \quad \text{(A14)}$$

In this last equation, the following identifications have been made. First, the total entropy flux is given by

$$J_T^S = J_L^S + J_n^S + J_p^S \equiv \frac{J_L^u}{T_L} + \frac{J_n^u}{T_n} + \frac{\nu_n J_n}{T_n} + \frac{J_p^u}{T_p} - \frac{\nu_p J_p}{T_p} \quad \text{(A15)}$$

second, the total energy absorbed from the incident light:

$$P = P_L + P_n + P_p \quad \text{(A16)}$$

and most important, the heat flux is defined along with the definition suggested by Muscato [16] as

$$J_q = J_L^u + J_n^u + J_p^u + \nu_n J_n - \nu_p J_p \quad \text{(A17)}$$

From the right hand side of Equation (A10) one gets the entropy production:

$$\sigma = \frac{J_n}{T} \cdot \nabla \hat{\phi}_n + \frac{J_p}{T} \cdot \nabla \hat{\phi}_p + J_q \cdot \nabla\left(\frac{1}{T}\right) + (R-G)\left(\frac{\nu_n + \nu_p}{T}\right) + \frac{P}{T} \quad \text{(A18)}$$

In this way, there exist five thermodynamic dissipative fluxes, namely, the electron (J_n) and hole (J_p) fluxes, the heat flux (J_q), the net generation-recombination of electron-hole pairs ($R-G$) and the energy being absorbed by the LEH system (P). The associated thermodynamic forces are: $\frac{1}{T}\nabla\hat{\phi}_n$, $-\frac{1}{T}\nabla\hat{\phi}_p$, $\nabla\left(\frac{1}{T}\right)$, $\frac{\nu_n + \nu_p}{T}$ and $\frac{1}{T}$, respectively.

We use the above definition of thermodynamic forces and fluxes to express the contributions to the total entropy production

$$\sigma = \sigma_{J_n} + \sigma_{J_p} + \sigma_{J_q} + \sigma_{RG} + \sigma_P \quad \text{(A19)}$$

with

$$\sigma_{J_n} = J_n\left(\frac{1}{T}\frac{\partial \nu_n}{\partial x} + \frac{q}{T}\frac{\partial \varphi}{\partial x}\right) \quad \text{(A20)}$$

$$\sigma_{J_p} = J_p\left(-\frac{1}{T}\frac{\partial \nu_p}{\partial x} - \frac{q}{T}\frac{\partial \varphi}{\partial x}\right) \quad \text{(A21)}$$

$$\sigma_{J_q} = J_q\frac{\partial}{\partial x}\left(\frac{1}{T}\right) \quad \text{(A22)}$$

$$\sigma_{RG} = \frac{R-G}{T}\left(\nu_p + \nu_n\right) \quad \text{(A23)}$$

$$\sigma_P = \frac{P}{T} \quad \text{(A24)}$$

Another consequence of the selection made of thermodynamic fluxes and forces is the Onsager's structure for the constitutive equations, which becomes

$$\begin{pmatrix} J_n \\ J_p \\ J_q \\ R-G \\ P \end{pmatrix} = \begin{pmatrix} L_{nn} & 0 & L_{nq} & 0 & 0 \\ 0 & L_{pp} & L_{pq} & 0 & 0 \\ L_{qn} & L_{qp} & L_{qq} & 0 & 0 \\ 0 & 0 & 0 & L_R & 0 \\ 0 & 0 & 0 & 0 & L_p \end{pmatrix} \begin{pmatrix} \dfrac{1}{T}\nabla\hat{\varphi}_n \\ \dfrac{1}{T}\nabla\hat{\varphi}_p \\ \nabla\dfrac{1}{T} \\ \dfrac{\nu_n+\nu_p}{T} \\ \dfrac{1}{T} \end{pmatrix} \qquad (A25)$$

All the zeros in the Onsager's matrix are a result of the fundamental assumption that fluxes and forces of different tensorial order do not couple. This is in agreement with Curie's principle which states that the dissipative fluxes do not depend on all the thermodynamic forces. We display, for completeness, the final form of the constitutive equations for fluxes with explicit expressions and values of the Onsager's *coefficients* to first order:

$$J_n = L_{11}\frac{\partial \nu_n}{\partial x} - L_{12}E_x - L_{13}\frac{\partial T}{\partial x} \qquad (A26)$$

$$J_p = -L_{21}\frac{\partial \nu_p}{\partial x} + L_{22}E_x - L_{23}\frac{\partial T}{\partial x} \qquad (A27)$$

$$J_q = L_{31}\frac{\partial \nu_n}{\partial x} - L_{33}\frac{\partial \nu_p}{\partial x} + \left(-L_{32}+L_{34}\right)E_x - L_{35}\frac{\partial T}{\partial x} \qquad (A28)$$

$$R-G = L_{41}\left(\nu_p+\nu_n\right) \qquad (A29)$$

$$P = L_{51}\frac{1}{T} \qquad (A30)$$

The coefficients L_{ij} are given by

$$L_{11} = g_n/q^2, \ L_{12} = g_n/q, \ L_{13} = g_nS_{ee}/q, \ L_{21} = g_p/q^2, \ L_{22} = g_p/q, \ L_{23} = g_pS_{ee}/q,$$

$$L_{31} = g_nT_0S_{ee}/q, \ L_{32} = g_nT_0S_{ee}, \ L_{33} = g_pT_0S_{ee}/q, \ L_{34} = g_pT_0S_{ee}, \ L_{35} = K$$

$$L_{41} = \left(\frac{C_nC_p}{C_n(n_0+n_1)+C_p(p_0+p_1)}\right)\left(\frac{n_0p_0}{K_BT_0}\right), \ L_{51} = 1 \qquad (A31)$$

where g_i are the electric conductivities of electrons and holes, respectively, S_{ee} the Seebeck coefficient, T_0 the reference temperature, K the thermal conductivity, n_0 and p_0 the density of electrons and holes at the reference temperature, respectively. K_B is Boltzmann's constant and q the electron electric charge. For numerical values of relevant coefficients see Appendix D. The selection of the coefficients L_{ij} has been made by addressing known phenomenological laws of thermoelectric phenomena. From the possible physical mechanisms causing the generation-recombination processes, we assume that only phonon transitions contribute to the determination of the coefficient L_{41} [23]. Accordingly with Shockley and Read's theory phonon transitions take place primarily in two steps by way of traps [21]. The constants C_n and C_p in the expression of L_{41} are the probability per unit time

that an electron in the conduction band will be captured by a trap and that a hole will be captured if the trap is filled with an electron so that it is in a condition to capture a hole, respectively. The quantities n_1 y p_1 are typical deviations of the particle densities from the reference states. We also assume that the photon transitions due to the incident light are proportional to the sum of chemical potentials $(v_p + v_n)$ [21].

The physical meaning of each term in equations (A26) to (A28) is well known [24]. We only mention that the third term on the r.h.s. of equations (A26) and (A27) corresponds to the Seebeck effect causing a flux of electrons and holes due to a temperature gradient, respectively, while in equation (A28) the third and the fourth terms describe the Peltier effect producing a heat flux due to the presence of an electric field. Moreover, Fourier and Fick laws are represented by the first terms on the r.h.s. of Equations (A26) and (A27).

The conservation and constitutive equations must be complemented with Poisson's equation:

$$\frac{\partial}{\partial x}\left(\varepsilon \frac{\partial \phi}{\partial x}\right) = q(n - p) \tag{A32}$$

which has been written here for undoped materials by taking the electric charge density as

$$\rho = q(p - n) \tag{A33}$$

We close this appendix with two additional points. The first is the use of the caloric equation for rewriting the total internal energy balance equation, obtained by summing Equations (A3)–(A5):

$$\rho_s C_v \frac{\partial T}{\partial t} + \frac{\partial J_q}{\partial x} = qE\left(J_p - J_n\right) + P \tag{A34}$$

where ρ_s is the volumetric mass density of the material, C_v the specific heat at constant volume, and T the local equilibrium temperature. There are two source terms in the temperature equation, namely, the first on the r.h.s. in the same equation due to the work made by the self-consistent electric field acting on the charged particles and the second is the absorbed energy from the incident light which is converted in heat. Secondly, the definition made of the heat flux, Equation (A17), differs from that of de Groot and Mazur [25], who defined it as

$$J_q = J_L^u + J_n^u + J_p^u \equiv J_T^u \tag{A35}$$

If one assumes this definition then Equation (A14) converts in

$$\frac{\partial S_T}{\partial t} + \nabla \cdot J_T^S = \frac{J_n}{T} \cdot \hat{\phi}_n - \frac{J_p}{T} \cdot \hat{\phi}_p + J_q \cdot \nabla\left(\frac{1}{T}\right) - \frac{1}{T} J_n \cdot \left(T\nabla \frac{v_n}{T}\right) - \frac{1}{T} J_p \cdot \left(T\nabla \frac{v_p}{T}\right) +$$
$$(R - G)\left(\frac{v_n + v_p}{T}\right) + \frac{P}{T}. \tag{A36}$$

This equation is in accordance with Equation (37) on page 343 of de Groot and Mazur. The last two terms on the r.h.s. do not appear in Equation (37) since conservation of total internal energy is assumed.

B. Optics

The term P, in Equation (A34) (defined in Equation (A16)), is calculated by means of a temporal average taken over many periods of oscillation of the incident light. The temporal average does not affect the other terms in Equation (A34) because they are slow varying variables. In fact, the motion of the free carriers (electrons and holes) is not significantly affected by the electric field of the incident radiation, and so the internal electric energy of the LEH system. In this respect, it must be mentioned that the characteristic time of the temperature t_T (that used to calculate the non-dimensional time) and that of the electric field of the incident light t_E (the inverse of light frequency) are related by $t_T / t_E = 10^{-6} / 10^{-14} = 10^8$. This means that the temperature is a slow thermodynamic variable compared with the fast changes of the electric field of the incident light arriving to a stationary profile not perturbed by the rapid oscillations of the electric field. The generation of internal energy P is then given by [15]:

$$P = \left\langle \frac{\partial S_{A1}}{\partial x} \right\rangle \tag{B1}$$

being S_{A1} the magnitude of the absorbed light energy in the medium. The symbol $\langle \ \rangle$ represents the time average taken over a big enough number of oscillations of the electric field of the incident light. It is defined as $\langle \bullet \rangle \equiv \underset{t \to \infty}{Lim} \int_0^t (\bullet) dt'$. In a physical sense the limit is taken until the stationary state has been reached. This occurs for $t > t_T$. Thus, $t \gg t_E$.

We now obtain the expression for the absorbed light intensity in the medium accordingly with Figure 10 where S_I is the incident light intensity, $S_{T1} = S_I T_{am}$ the transmitted light intensity in the air-medium interface, $S'_{T1}(x) = S_{T1} e^{-\alpha x}$ the distribution of the intensity of the light propagated to the interface medium-air which is attenuated by the medium (it is a function of the position), $S_{R2}(x) = S'_{T1} R_{ma}$ the intensity of the reflected light at the interface medium-air and $S'_{R2}(x) = S_{R2} e^{-\alpha(x-L)}$ the intensity of the light propagated to the interface air-medium which is attenuated by the medium. α is the absorption coefficient of the medium. T_{am} is the transmission coefficient in the interface air-medium and R_{ma} is the reflection coefficient in the interface medium-air. Finally, the absorbed energy in the medium is obtained when one substitutes the previous expressions in the following and takes the spatial derivative:

$$S_{A1}(x) = S_{T1} - S'_{T1}(x) + S_{R2}(x) - S'_{R2}(x)$$

The result for the first step reads:

$$S_{A1}(x) = S_I T_{am} \left(1 - e^{-\alpha x} \left(1 - R_{ma} \left(1 - e^{-\alpha(x-L)} \right) \right) \right). \tag{B2}$$

Thus, the explicit expression for P becomes

$$P(x) = \alpha T_{am} S_I \left(e^{-\alpha x} + R_{ma} e^{-\alpha(x-L)} \right) \tag{B2}$$

The term G, in Equations (A1) and (A2), is given by

$$G(x) = \frac{\alpha S_I}{hf} \left(S_{T1} - S_{A1}(x) \right) \tag{B4}$$

with h the Planck constant and f the light frequency. The transmission and reflection coefficients at the interfaces air-material and material-air are

$$T_{am} = \frac{n_m}{n_a}\left(\frac{2n_a}{n_m + n_a}\right)^2 \qquad (B5)$$

and

$$R_{ma} = \left(\frac{n_a - n_m}{n_a + n_m}\right)^2 \qquad (B6)$$

respectively. n_m is the refractive index of the material and n_a that of air.
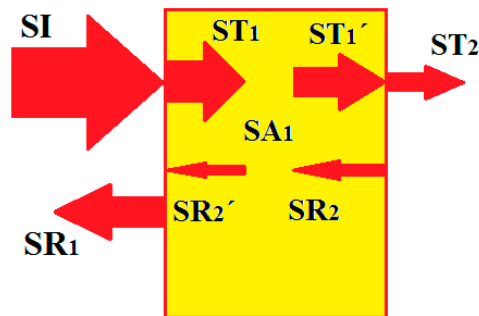
Figure 10. Schematic of the transmitted, attenuated and reflected light in the medium which were considered for calculating the absorbed energy S_{A1}.

C. Dimensional Analysis

The complexity of Equations (A1), (A2) and (A34) can be reduced through a dimensional analysis. This is achieved by making the usual transformation:

$$x^* = \frac{x}{L}, \quad t^* = \frac{t}{\tau}, \qquad n^* = \frac{n}{n_0}, \qquad p^* = \frac{p}{p_0}, \qquad T^* = \frac{T}{T_0} \qquad (C1)$$

and the potential function of the self-consistent electric field transformed as

$$\phi^* = \frac{\varepsilon}{qn_0 L^2}\phi \qquad (C2)$$

We begin the analysis of the dissipative fluxes, Equations (A26)–(A28). It can be proved that in the case of the heat flux (A28) all the terms are $O(10^{-11})$ or smaller, excepting the term in the coefficient L_{35} which is $O(10^0)$. Therefore, we have conserved only this last term in the calculations. The heat flux takes the Fourier law form

$$J_q = -L_{35}\frac{\partial T}{\partial x} \qquad (C3)$$

In this way the temperature equation takes the dimensional form

$$\rho_s C_v \frac{\partial T}{\partial t} - L_{35}\frac{\partial^2 T}{\partial x^2} = P \qquad (C4)$$

As it can be seen, the temperature equation is of the diffusion type with a source term coming from the interaction of the incident light with the medium. We now consider the particle fluxes, Equations (A26) and (A27). Dimensional analysis shows that the terms in the self-consistent electric field can be neglected with respect to the terms in the chemical potentials. In this way, the constitutive equations for the particle fluxes become

$$J_n = L_{11} \frac{\partial v_n}{\partial x} - L_{13} \frac{\partial T}{\partial x} \tag{C5}$$

$$J_p = -L_{21} \frac{\partial v_p}{\partial x} - L_{23} \frac{\partial T}{\partial x} \tag{C6}$$

With the above simplifications and neglecting lowest order terms the dimensional Equations (A1) and (A2) read, for the electron density,

$$\frac{\partial n}{\partial t} + \frac{K_B L_{11} T(x)}{n(x)^2} \left(\frac{\partial n}{\partial x} \right)^2 - \frac{2K_B L_{11}}{n(x)} \frac{\partial T}{\partial x} \frac{\partial n}{\partial x} - \frac{K_B L_{11} T(x)}{n(x)} \frac{\partial^2 n}{\partial x^2} +$$
$$\left(L_{13} - K_B L_{11} Log(n) \right) \frac{\partial^2 T}{\partial x^2} + R(x) - G(x) = 0 \tag{C7}$$

A similar equation is obtained for the hole density:

$$\frac{\partial p}{\partial t} + \frac{K_B L_{21} T(x)}{p(x)^2} \left(\frac{\partial p}{\partial x} \right)^2 - \frac{2K_B L_{21}}{p(x)} \frac{\partial T}{\partial x} \frac{\partial p}{\partial x} - \frac{K_B L_{21} T(x)}{p(x)} \frac{\partial^2 p}{\partial x^2} -$$
$$\left(L_{23} + K_B L_{21} Log\left(\frac{p}{N_v} \right) \right) \frac{\partial^2 T}{\partial x^2} + R(x) - G(x) = 0. \tag{C8}$$

It is worth noting that the temperature equation becomes decoupled from Equations (C7) and (C8). The final form of Equations (C7)–(C8) in the stationary state used in the calculations is shown in Equations (1) and (2) in Section 2.2.

D. Constants

In this final appendix the values of the constants in the solutions of temperature and particle densities, Equations (9)–(11), can be found. Units are omitted.

For Silicon:

$$k_{0T} = 1.1, \ k_{1T} = -3.384 \times 10^{-10}, \ k_{2T} = -2.318 \times 10^{-10}, \ k_{3T} = -6.209 \times 10^{-10}, \ a = 1,$$
$$b = 0.5, \ L_{11} = 9.747 \times 10^{33}, \ L_{13} = 6.862 \times 10^{11}, \ L_{21} = 1.347 \times 10^{33}, \ L_{23} = 9.484 \times 10^{10},$$
$$L_{35} = 148, \ L_{41} = 1.55 \times 10^{34}$$

For Germanium:

$$k_{0T} = 1.1, \ k_{1T} = -2.96 \times 10^{-13}, \ k_{2T} = -1.01 \times 10^{-14}, \ k_{3T} = -1.965 \times 10^{-9}, \ a = 7, \ b = 3.5,$$
$$L_{11} = 6.257 \times 10^{37}, \ L_{13} = 1.502 \times 10^{15}, \ L_{21} = 1.859 \times 10^{37}, \ L_{23} = 4.461 \times 10^{14}, \ L_{35} = 59.9,$$
$$L_{41} = 1.17 \times 10^{38}$$

References

1. Estrada-Wiese, D.; del Río, J.A.; de la Mora, M.B. Heat transfer in photonic mirrors. *J. Mater. Sci.* **2014**, *25*, 4348–4355.
2. Boggi, S.; Razzitte, A.C.; Fano, W.G. Non-equilibrium thermodynamics and entropy production spectra: A tool for the characterization of ferromagnetic materials. *J. Non-Equilib. Thermodyn.* **2013**, *38*, 175–183.
3. Vázquez, F.; del Río, J.A. Thermodynamic characterization of the diffusive transport to wave propagation transition in heat conducting thin films. *J. Appl. Phys.* **2012**, *112*, 123707.
4. Figueroa, A.; Vázquez, F. Optimal performance and entropy generation transition from micro to nanoscaled thermoelectric layers. *Int. J. Heat Mass Transf.* **2014**, *71*, 724–731.
5. Lucia, U. Stationary open systems: A brief review on contemporary theories on irreversibility. *Physica A* **2013**, *392*, 1051–1062.
6. Goupil, C.; Seifert, W.; Zabrocki, K.; Müller, E.; Snyder, G.J. Thermodynamics of Thermoelectric Phenomena and Applications. *Entropy* **2011**, *13*, 1481–1517.
7. Maldovan, M. Narrow Low-Frequency Spectrum and Heat Management by Thermocrystals. *Phys. Rev. Lett.* **2013**, *110*, 025902.
8. Yilbas B.S.; Al-Dweik A.Y. Short-pulse heating and analytical solution to non-equilibrium heating process. *Physica B* **2013**, *417*, 28–32.
9. Mansoor, S.B.; Yilbas, B.S. Laser short-pulse heating of silicon-aluminum thin films. *Opt. Quant. Electron.* **2011**, *42*, 601–618.
10. Lewandowska, M.; Malinowski, L. An analytical solution of the hyperbolic heat conduction equation for the case of a finite medium symmetrically heated on both sides. *Int. Commun. Heat Mass Transf.* **2006**, *33*, 61–69.
11. Barbagiovanni, E.G.; Loockwood, D.J.; Simpsom, P.J.; Goncharova, L.V. Quantum confinement in Si and Ge nanostructures: Theory and experiment. *Appl. Phys. Rev.* **2014**, *1*, 011302; doi:10.1063/1.4835095.
12. Zhao, S.; Yedlin, M.J. A new Iterative Chebyshev Spectral Method for Solving the Elliptic Equation $\nabla \cdot (\sigma \nabla u) = f$. *J. Comput. Phys.* **1994**, *113*, 215–223.
13. Peyret, R. *Spectral Methods for Incompressible Viscous Flow*, 5th ed.; Springer: New York, NY, USA, 2002.
14. Joshi, A.A.; Majumdar, A. Transient ballistic and diffusive phonon heat transport in thin films. *J. Appl. Phys.* **1993**, *74*, 31–39.
15. Wachutka, G.K. Rigorous thermodynamic treatment of heat generation and conduction in semiconductor device modeling. *IEEE Trans. Comput. Aided Des.* **1990**, *9*, 1141–1149.
16. Muscato, O. The Onsager reciprocity principle as a check of consistency for semiconductor carrier transport models. *Physica A* **2001**, *289*, 422–458.
17. Chen, W.H.; Wang, C.-C.; Hung, C.-I.; Yang, C.-C.; Juang, R.-C. Modeling and simulation for the design of thermal-concentrated solar thermoelectric generator. *Energy* **2014**, *64*, 287–297.
18. Gupta, M.P.; Sayer, M.-H.; Mukhopadhyay, S.; Kumar, S. Ultrathin Thermoelectric Devices for On-Chip Peltier Cooling. *IEEE Trans. Compon. Packag. Manuf. Technol.* **2011**, *1*, 1395–1405.

19. Singh, A.; Avasthi, D.V.; Singh, T.; Kumar, D. Design a Thermophotovoltaic System to Optimize Surface Radiative conductive heat flux. *Int. J. Emerg. Trends Eng. Dev.* **2014**, *4*, 216–222.

20. Muscato, O.; di Stefano, V. Hydrodynamic simulation of a $n^+ - n - n^+$ Silicon nanowire. *Contin. Mech. Thermodyn.* **2014**, *26*, 197–205.

21. Selberherr, S. *Analysis and Simulation of Semiconductor Devices*; Springer: Vienna, Austria, 1984.

22. Jou, D.; Casas-Vázquez, J.; Lebon, G. *Extended Irreversible Thermodynamics*, 4th ed.; Springer: New York, NY, USA; Dordrecht, The Netherlands; Heidelberg, Germany; London, UK, 2001.

23. Shockley, W.; Read, W.T. Statistics of the recombinations of holes and electrons. *Phys. Rev.* **1952**, *87*, 835–842.

24. Sellito, A.; Cimmelli, V.; Jou, D. Thermoelectric effects and size dependency of the figure-of-merit in cylindrical nanowires. *Int. J. Heat Mass Transf.* **2013**, *57*, 109–116.

25. De Groot, S.R.; Mazur, P. *Non-Equilibrium Thermodynamics*; Dover: New York, NY, USA, 1984.